Progress In Electromagnetics Research M, Vol. 88, 53–63, 2020

Computation of Electric and Magnetic Field Distribution inside a Multilayer Cylindrical Conductor

Slavko Vujević, Dino Lovrić*, Ivan Krolo, and Ilijana Duvnjak

Abstract—In this paper, a numerical algorithm for computation of electric and magnetic fields inside a multilayer cylindrical structure with an arbitrary number of homogeneous layers is presented. Each layer can have arbitrary value of electrical conductivity, permeability, and permittivity. Theoretical background of the model is based on Maxwell equations where modified Bessel functions have been chosen for solution formulas. Modified Bessel functions are also scaled to avoid underflow/overflow issues. This results in a numerically robust and highly accurate numerical algorithm for computation of electric and magnetic fields inside a multilayer conductor. Using the derived expression for electric field on the surface of the conductor, the formula for per-unit-length internal impedance of the general multilayer cylindrical conductor is also obtained.

1. INTRODUCTION

In analysis of various electromagnetic phenomena, it is necessary in some cases to accurately obtain the distribution of the electric and magnetic fields present in a current carrying conductor. For example, this is important in transient electromagnetic analysis where higher frequency currents flow along the conductor and skin effect becomes more prominent [1]. Using the fields on the surface of the conductor, one can then compute the internal impedance or surface impedance as it is sometimes referred to. In the available literature, most authors analyze homogeneous single-layer conductors [2–6], in some cases two-layer conductors [7, 8], and some consider multilayer conductors [9–11]. In the case of cylindrical multilayer structures, the authors in [9–11] utilize a cascade of two-port networks to model a multilayer structure. The problem that occurs with this approach lies in the inherent numerical instability present in the transfer matrix of the system, where some elements of the matrix tend to infinity for high frequencies even for extra thin layers. To circumvent this, the authors are forced to subdivide the layers into a large number of fictive sublayers.

In this paper, a different approach to model multilayer structures will be presented, which is both numerically robust and highly accurate. In addition, the proposed algorithm features a smaller number of unknowns than those in [9–11]. In the numerical algorithm proposed in this paper, a multilayer cylindrical structure consisting of an arbitrary number of layers is considered. Each layer of the multilayer conductor is considered to be linear, isotropic and homogeneous and characterized by arbitrary values of electrical conductivity, permeability and permittivity. The first layer of the multilayer conductor can be either a tubular layer or a solid layer which slightly changes the subsequent linear system of equations.

Theoretical background of the presented numerical algorithm is derived directly from Maxwell equations. Displacement currents have been taken into account in all layers although their effect is negligible in layers with good conductance. Although the solutions of Maxwell equations can be written

Received 17 October 2019, Accepted 20 December 2019, Scheduled 3 January 2020

* Corresponding author: Dino Lovrić (dlovric@fesb.hr).

The authors are with the Faculty of Electrical Engineering, Mechanical Engineering and Naval Architecture, University of Split, Ruđera Boškovića 32, HR-21000 Split, Croatia.

using various special functions such as Bessel functions of the first and second kind, modified Bessel functions of the first and second kind or a combination of Bessel and modified Bessel functions [12–14], in this paper solutions based on modified Bessel functions have been chosen. This is because solutions based on modified Bessel function are numerically the most stable solutions of the field formulas especially for larger function arguments, which generally occur at higher frequencies. This was also discussed in papers [6, 7]. Furthermore, the chosen modified Bessel functions have been scaled up or down thus adding to the numerical stability of the numerical algorithm especially for larger function arguments.

In the presented numerical algorithm, a linear system of equations is formed from the boundary conditions between layers and on the edges of the multilayer conductor. The number of equations is always the double of the number of layers in the multilayer conductors which is significantly less than in the case of models based on a cascade of two-port networks. Furthermore, in the presented model, when the unknowns are computed, one can then compute electric and magnetic fields in any observation point directly, which is not the case in for example [11].

The accuracy of the presented numerical algorithm has been validated by comparing the computation of per-unit-length internal impedance to the authors' closed-form expressions of a two-layer conductor [7]. Furthermore, comparison of per-unit-length internal impedance has also been made with the model based on a cascade of two-port networks presented in [11] where good agreement was found. Also, in this paper, the formula for computing the per-unit-length internal impedance is given, which is derived from the electric field on the surface of the multilayer conductor.

2. OVERVIEW OF THE MODEL OF THE MULTILAYER CYLINDRICAL CONDUCTOR

The multilayer cylindrical conductor considered in this paper can consist of an arbitrary number of layers. Let the total number of layers be m.

An arbitrary ith layer is characterized by its external radius r_i whereas the internal radius of the ith layer is determined by the external radius of the adjacent layer $i-1$. Furthermore, as for the electrical properties of the layer, the arbitrary ith layer is described by its electrical conductivity σ_i, magnetic permeability μ_i and permittivity ε_i.

In the presented numerical algorithm, the innermost layer of the multilayer conductor (the first layer) can be either a solid cylindrical conductor or a tubular cylindrical conductor. If the first layer is solid conductor, then $r_0 = 0$, whereas if it is a tubular conductor, then $r_0 \neq 0$. In Figure 1, these two cases are depicted.

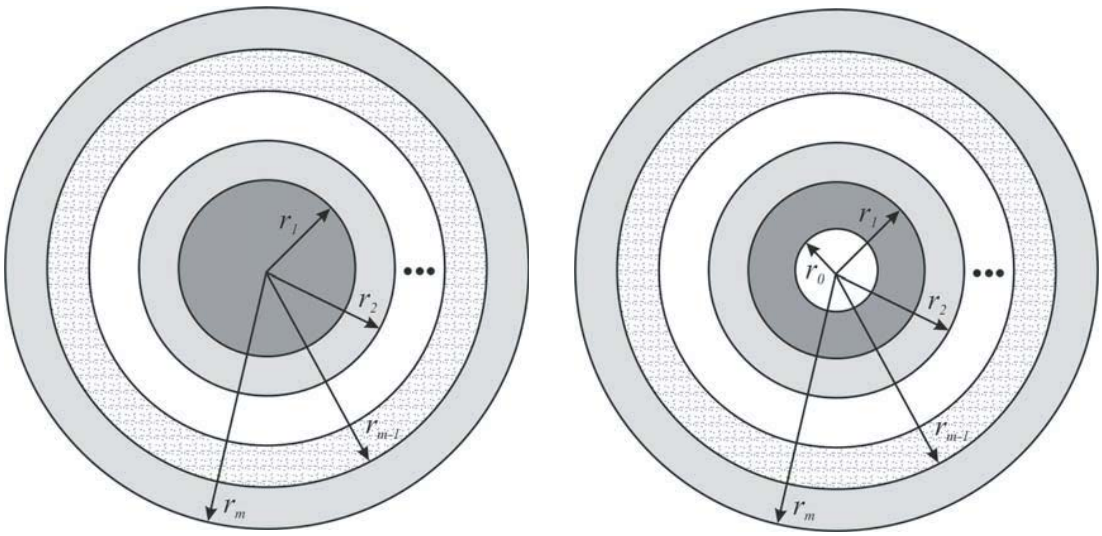

Figure 1. Solid and tubular multilayer cylindrical conductors possible in the presented model.

3. COMPUTATION OF ELECTRIC AND MAGNETIC FIELD IN THE MULTILAYER CONDUCTOR

Formulas for computation of electric and magnetic fields inside an arbitrary ith layer are derived directly from Maxwell equations. Each layer of the multilayer conductor is considered to be linear, isotropic and homogeneous. Although the solutions of Maxwell equations for magnetic and electric fields of the ith layer can be written using various special functions, the most numerically stable solutions have proven to be those based on modified Bessel functions [6, 7]. This is especially true for large function arguments as shown in [6, 7]. Expressions for magnetic and electric fields inside an arbitrary ith layer of the multilayer conductor used om this paper are:

$$\bar{H}_i = \bar{I}_{tot} \cdot \left[\bar{C}_i \cdot \bar{I}_1\left(\bar{\gamma}_i \cdot r\right) + \bar{D}_i \cdot \bar{K}_1\left(\bar{\gamma}_i \cdot r\right)\right] \tag{1}$$

$$\bar{E}_i = \frac{\bar{I}_{tot} \cdot \bar{\gamma}_i}{\bar{\kappa}_i} \cdot \left[\bar{C}_i \cdot \bar{I}_0\left(\bar{\gamma}_i \cdot r\right) - \bar{D}_i \cdot \bar{K}_0\left(\bar{\gamma}_i \cdot r\right)\right] \tag{2}$$

where $\bar{I}_0$ is the complex-valued modified Bessel function of the first kind of order zero; $\bar{K}_0$ is the complex-valued modified Bessel function of the second kind of order zero; $\bar{I}_1$ is the complex-valued modified Bessel function of the first kind of order one; $\bar{K}_1$ is the complex-valued modified Bessel function of the second kind of order one [14]; $\bar{C}_i$ and $\bar{D}_i$ are the unknown complex-valued coefficients for the ith layer; $\bar{\kappa}_i = \sigma_i + j \cdot \omega \cdot \varepsilon_i$ is the complex conductivity of the ith layer; σ_i is the conductivity of the ith layer; ε_i is the permittivity of the ith layer; ω is the circular frequency of the multilayer conductor current; j is the imaginary unit; and $\bar{I}_{tot}$ represents the phasor of the total harmonic conductor current.

The complex wave propagation constant of the ith layer is defined by the following general equation:

$$\bar{\gamma}_i = \alpha_i + j \cdot \beta_i = \sqrt{\frac{\omega \cdot \mu_i}{2}} \cdot \left(\frac{\sigma_i}{N_i} + j \cdot N_i\right) \tag{3}$$

$$N_i = \sqrt{\omega \cdot \varepsilon_i + \sqrt{\left(\omega \cdot \varepsilon_i\right)^2 + \sigma_i^2}} \tag{4}$$

where μ_i is the magnetic permeability of the ith layer of the multilayer conductor.

In order to achieve a more stable computation, modified Bessel functions as well as the unknown complex coefficients are scaled up or down to achieve a similar order of magnitude according to the following expressions [6, 7]:

$$\bar{I}_0\left(\bar{\gamma}_i \cdot r\right) = e^{\bar{\gamma}_i \cdot r} \cdot \bar{I}_0^s\left(\bar{\gamma}_i \cdot r\right); \qquad \bar{I}_1\left(\bar{\gamma}_i \cdot r\right) = e^{\bar{\gamma}_i \cdot r} \cdot \bar{I}_1^s\left(\bar{\gamma}_i \cdot r\right) \tag{5}$$

$$\bar{K}_0\left(\bar{\gamma}_i \cdot r\right) = e^{-\bar{\gamma}_i \cdot r} \cdot \bar{K}_0^s\left(\bar{\gamma}_i \cdot r\right); \qquad \bar{K}_1\left(\bar{\gamma}_i \cdot r\right) = e^{-\bar{\gamma}_i \cdot r} \cdot \bar{K}_1^s\left(\bar{\gamma}_i \cdot r\right) \tag{6}$$

$$\bar{C}_i = e^{-\bar{\gamma}_i \cdot r_i} \cdot \bar{C}_i^s; \qquad \bar{D}_i = e^{\bar{\gamma}_i \cdot r_{i-1}} \cdot \bar{D}_i^s \tag{7}$$

Introducing the scaled values of modified Bessel functions and unknown coefficients into Eqs. (1) and (2), the following equations for electric and magnetic fields inside the ith layer are obtained:

$$\bar{H}_i = \bar{I}_{tot} \cdot \left[\bar{C}_i^s \cdot \bar{I}_1^s\left(\bar{\gamma}_i \cdot r\right) \cdot e^{-\bar{\gamma}_i \cdot \left(r_i - r\right)} + \bar{D}_i^s \cdot \bar{K}_1^s\left(\bar{\gamma}_i \cdot r\right) \cdot e^{-\bar{\gamma}_i \cdot \left(r - r_{i-1}\right)}\right] \tag{8}$$

$$\bar{E}_i = \frac{\bar{I}_{tot} \cdot \bar{\gamma}_i}{\bar{\kappa}_i} \cdot \left[\bar{C}_i^s \cdot \bar{I}_0^s\left(\bar{\gamma}_i \cdot r\right) \cdot e^{-\bar{\gamma}_i \cdot \left(r_i - r\right)} - \bar{D}_i^s \cdot \bar{K}_0^s\left(\bar{\gamma}_i \cdot r\right) \cdot e^{-\bar{\gamma}_i \cdot \left(r - r_{i-1}\right)}\right] \tag{9}$$

The unknown scaled complex-valued coefficients $\bar{C}_i^s$ and $\bar{D}_i^s$ $(i = 1, 2, \ldots, m)$ are needed to accurately compute the distribution of the electric and magnetic fields inside the multilayer conductor. These $2 \cdot m$ unknown coefficients are computed from the boundary conditions between layers as well as on the edges of the conductor. Two cases are possible since the first layer can be either a solid layer or a tubular layer.

3.1. Computation of Unknown Complex-Valued Coefficients

Since there are a total of $2 \cdot m$ unknown scaled complex-valued coefficients $\bar{C}_i^s$ and $\bar{D}_i^s$ $(i = 1, 2, \ldots, m)$ one needs to form a set of $2 \cdot m$ linear equations. These equations are formed from the boundary conditions between layers and the boundary conditions on the edges of the conductor.

The first $2 \cdot (m-1)$ equations are formed from the boundary conditions between layers requiring that the tangential components of electric field intensity and magnetic field intensity are continuous on the border between two adjacent layers:

$$\overline{H}_i\big|_{r=r_i} = \overline{H}_{i+1}\big|_{r=r_i}; \qquad i = 1, 2, \ldots, m-1 \tag{10}$$

$$\overline{E}_i\big|_{r=r_i} = \overline{E}_{i+1}\big|_{r=r_i}; \qquad i = 1, 2, \ldots, m-1 \tag{11}$$

Equations (10)–(11) are valid for both the cases of a solid and tubular multilayer cylindrical conductor.

One additional equation, also valid for both the case of a solid and tubular cylindrical conductor, is derived from the boundary condition on the outer edge of the multilayer cylindrical conductor:

$$\bar{H}_m\big|_{r=r_m} = \frac{\bar{I}_{tot}}{2 \cdot \pi \cdot r_m} \tag{12}$$

The last equation in the system of equations is different for the cases of solid and tubular cylindrical conductors since it is derived from the innermost edge of the conductor (if it exists).

If a **solid** cylindrical conductor is considered, then the internal radius of the first layer equals zero ($r_0 = 0$). In this case, the field distribution in the first layer must yield physically valid results even if the observation point is situated in the center of the conductor ($r = 0$). However, modified Bessel functions of the second kind tend to infinity if their argument is zero which is not physically valid. To prevent this from happening, in the case of a solid cylindrical conductor, $\bar{D}_1^s$ must be chosen to equal zero, so the last equation in the system of equations for the case of the solid cylindrical conductor is:

$$\overline{D}_1^s = 0 \tag{13}$$

However, if a **tubular** cylindrical conductor is considered, then the internal radius of the first layer does not equal zero ($r_0 \neq 0$). In this case, there are no singularity issues as in the previous case, so the boundary condition on the innermost edge of the conductor can be included as the last equation in the system of equations for the tubular cylindrical conductor:

$$\overline{H}_1\big|_{r=r_0} = 0 \tag{14}$$

Therefore, introducing equations for electric and magnetic fields of Eqs. (8)–(9) into Eqs. (10)–(14), the following system of equations is obtained:

First $2 \cdot (\mathbf{m-1})$ equations:

$$\overline{C}_i^s \cdot \overline{I}_1^s(\bar{\gamma}_i \cdot r_i) + \overline{D}_i^s \cdot \overline{K}_1^s(\bar{\gamma}_i \cdot r_i) \cdot \bar{\nu}_i - \overline{C}_{i+1}^s \cdot \overline{I}_1^s(\bar{\gamma}_{i+1} \cdot r_i) \cdot \bar{\nu}_{i+1} - \overline{D}_{i+1}^s \cdot \overline{K}_1^s(\bar{\gamma}_{i+1} \cdot r_i) = 0; \quad i = 1, 2, \ldots, m-1 \tag{15}$$

$$\frac{\bar{\gamma}_i}{\bar{\kappa}_i} \cdot \left[\overline{C}_i^s \cdot \overline{I}_0^s(\bar{\gamma}_i \cdot r_i) - \overline{D}_i^s \cdot \overline{K}_0^s(\bar{\gamma}_i \cdot r_i) \cdot \bar{\nu}_i\right] - \frac{\bar{\gamma}_{i+1}}{\bar{\kappa}_{i+1}} \cdot \left[\overline{C}_{i+1}^s \cdot \overline{I}_0^s(\bar{\gamma}_{i+1} \cdot r_i) \cdot \bar{\nu}_{i+1} - \overline{D}_{i+1}^s \cdot \overline{K}_0^s(\bar{\gamma}_{i+1} \cdot r_i)\right] = 0; \quad i = 1, 2, \ldots, m-1 \tag{16}$$

Equation $2 \cdot \mathbf{m} - \mathbf{1}$:

$$\overline{C}_m^s \cdot \overline{I}_1^s(\bar{\gamma}_m \cdot r_m) + \overline{D}_m^s \cdot \overline{K}_1^s(\bar{\gamma}_m \cdot r_m) \cdot \bar{\nu}_m = \frac{1}{2 \cdot \pi \cdot r_m} \tag{17}$$

Equation $2 \cdot \mathbf{m}$:

- for a solid conductor:

$$\overline{D}_1^s = 0 \tag{18}$$

- for a tubular conductor:

$$\overline{C}_1^s \cdot \overline{I}_1^s(\bar{\gamma}_1 \cdot r_0) \cdot \bar{\nu}_1 + \overline{D}_1^s \cdot \overline{K}_1^s(\bar{\gamma}_1 \cdot r_0) = 0 \tag{19}$$

In Equations (15)–(19), the auxiliary scaling constant $\bar{\nu}_i$ equals:

$$\bar{\nu}_i = e^{-\bar{\gamma}_i \cdot (r_i - r_{i-1})} \tag{20}$$

By numerically solving the completely formed system of equations, all the unknown scaled complex-valued coefficients $\bar{C}_i^s$ and $\bar{D}_i^s$ $(i = 1, 2, \ldots, m)$ are obtained. In the presented numerical algorithm, the linear system of equations is solved using LAPACK LU decomposition routine with a high degree of accuracy. This was confirmed on a number of conductor configurations by substituting the computed coefficients into the Equations (15)–(19) and testing whether the right sides of the equations are all zero except in the case of Equation (17). The computed results were accurate to the 17th decimal place in the worst cases.

Now when $2 \cdot m$ coefficients are known, the distribution of electric field intensity and magnetic field intensity in any layer of the multilayer conductor can be computed using Equations (8)–(9) by introducing the now known complex-valued coefficients $\bar{C}_i$ and $\bar{D}_i$ for that layer.

4. COMPUTATION OF PER-UNIT-LENGTH INTERNAL IMPEDANCE

Per-unit-length internal impedance of the cylindrical multilayer conductor can be computed using the electric field on the surface of the multilayer cylindrical conductor using the following expression:

$$\bar{Z} = \frac{\bar{E}_i\big|_{r=r_m}}{\bar{I}_{tot}} \tag{21}$$

Introducing Eq. (8) into Eq. (21), the following equation for per-unit-length internal impedance of the multilayer conductor is obtained:

$$\bar{Z} = \frac{\bar{\gamma}_m}{\bar{\kappa}_m} \cdot \left[\bar{C}_m^s \cdot \bar{I}_0^s\left(\bar{\gamma}_m \cdot r_m\right) - \bar{D}_m^s \cdot \bar{K}_0^s\left(\bar{\gamma}_m \cdot r_m\right) \cdot \bar{\nu}_m\right] \tag{22}$$

5. DISCUSSION

By observing Equations (15)–(20), it can be easily deduced that the coefficients of the system of linear equations cannot tend to infinity as the frequency increases. This is a direct consequence of choosing the right general solution for electric and magnetic fields of Eqs. (8)–(9), which ensures numerical stability in all cases. The key quantity that ensures numerical stability in the coefficients of the linear system of equations is the quantity $\bar{\nu}_i$, described by (20) which for high frequencies tends to zero. However, in the case of algorithms based on a cascade of two-port networks, this is not the case because some coefficients of the transfer matrix, even for thin millimetre layers, tend to infinity for high frequencies, which is visible from Equations (27)–(30) given in [11]. It is evident that these equations contain both the quantity $\bar{\nu}_i$ but also the quantity $1/\bar{\nu}_i$, which for high frequencies tends to infinity. Scaling the modified Bessel function [11] cannot help with the numerical stability in this case. To circumvent these problems, these kinds of algorithms must subdivide layers into a multitude of fictive sublayers to ensure that the quantity $1/\bar{\nu}_i$ does not become too large or tend to infinity. The same problem exists in approach [10], but in this case this is not immediately visible because unscaled Bessel and modified Bessel functions are used which produces additional numerical instabilities at higher frequencies.

The numerical algorithm presented in this paper has no need for fictive sublayers and it requires in all cases the computation of $2 \cdot m$ unknown coefficients. Afterwards, electric and magnetic fields can be computed in all points of the multilayer conductor using Eqs. (8)–(9). However, algorithms based on a cascade of two-port networks [9–11] have significantly more unknowns, and electric and magnetic fields are computed only on the boundaries of fictive layers

6. NUMERICAL EXAMPLES

6.1. Validation of the Model

The model of the multilayer conductor presented in this paper has been compared to the model for computation of per-unit length internal impedance of two-layer conductors published in [7]. In the

model presented in [7], there is no system of equations that needs to be solved since analytical formulas are provided. The two compared models yield identical results for any combination of parameters of conductive layers and for any frequency of the time-harmonic current.

6.2. Comparison with the Model Based on a Cascade of a Set of Two-Port Networks [11]

In the second example, the presented model of the multilayer conductor has been compared to a model of a multilayer conductor which is based on a set of two-port networks [11]. In the model presented in [11] the conductor is subdivided into a number of two-port networks with the unknowns being the electric and magnetic fields on each of the sublayers (this yields more unknowns). The conductor considered for comparison is a two layer conductor as in [11]: the first layer is an layer made of stainless steel ($r_1 = 1\,\text{mm}$, $\sigma_1 = 1.37\,\text{MS/m}$, $\mu_1 = 1.02 \cdot \mu_0$, $\varepsilon_1 = \varepsilon_0$) and the second layer is a copper layer ($r_2 = 3\,\text{mm}$, $\sigma_2 = 59.6\,\text{MS/m}$, $\mu_2 = 0.999994 \cdot \mu_0$, $\varepsilon_2 = \varepsilon_0$).

Only the internal impedance values on the outer edge of conductor are available for comparison, so in Table 1 the comparison is made of the conductor internal resistance per-unit-length, whereas in Table 2 the comparison is made of the conductor internal inductance per-unit-length. As can be seen from the computed results, there are slight differences for the per-unit-length inductance where the maximum percent difference between the results is 0.016% for lower frequency values. It is important to note that the algorithm presented in [11] requires the addition of 109 fictive sublayers to circumvent the previously discussed numerical stability issues present in the transfer matrix.

Table 1. Comparison of per-unit length internal resistance computed by the presented algorithm and algorithm from [11].

f	R with 109 sublayers [11]	R proposed
Hz	Ω/m	Ω/m
10	0.000666	$0.6656835439108669 \cdot 10^{-3}$
10^1	0.000666	$0.6656864441237284 \cdot 10^{-3}$
10^2	0.000666	$0.6659763814720126 \cdot 10^{-3}$
10^3	0.000694	$0.6941563020524239 \cdot 10^{-3}$
10^4	0.001529	$0.1528670732671533 \cdot 10^{-2}$
10^5	0.004470	$0.4469882840089542 \cdot 10^{-2}$
10^6	0.013803	$0.1380338766464217 \cdot 10^{-1}$
10^7	0.043326	$0.4332592082623524 \cdot 10^{-1}$
10^8	0.136687	$0.1366867194241476 \cdot 10^{0}$
10^9	0.43920	$0.4319202312891782 \cdot 10^{0}$
10^{10}	1.365531	$0.1365530811214155 \cdot 10^{1}$
10^{11}	4.317867	$0.4317866941434107 \cdot 10^{1}$
10^{12}	13.653966	$0.1365397910870375 \cdot 10^{2}$

6.3. Solid Multilayer Conductor — Computation of Distribution of Electric and Magnetic Fields and Per-Unit-Length Internal Impedance

A solid four-layer conductor is observed in this numerical example. The first layer is an iron layer ($r_1 = 5\,\text{mm}$, $\sigma_1 = 10\,\text{MS/m}$, $\mu_1 = 5000 \cdot \mu_0$, $\varepsilon_1 = \varepsilon_0$), the second layer is a copper layer ($r_2 = 10\,\text{mm}$, $\sigma_2 = 59.6\,\text{MS/m}$, $\mu_2 = \mu_0$, $\varepsilon_2 = \varepsilon_0$), the third layer is air ($r_3 = 15\,\text{mm}$, $\varepsilon_3 = \varepsilon_0$, $\mu_3 = \mu_0$), whereas the fourth layer is a lead layer ($r_4 = 20\,\text{mm}$, $\sigma_4 = 4.55\,\text{MS/m}$, $\mu_4 = \mu_0$, $\varepsilon_4 = \varepsilon_0$).

Using the previously outlined numerical algorithm, which was implemented into a FORTRAN program, distribution of electric and magnetic fields is computed in 1000 observation points inside the observed conductor for chosen frequency values (0.1 Hz, 1 Hz, 10 Hz, 100 Hz, and 1000 Hz). The results

Table 2. Comparison of per-unit length internal inductance computed by the presented algorithm and algorithm from [11].

f	L with 109 sublayers [11]	L proposed
Hz	nH/m	H/m
10	41.10868	$0.4111536584244416 \cdot 10^{-7}$
10^1	41.10860	$0.4111528942512286 \cdot 10^{-7}$
10^2	41.10097	$0.4110765005949085 \cdot 10^{-7}$
10^3	40.36059	$0.4036663500536945 \cdot 10^{-7}$
10^4	21.58939	$0.2158919403031265 \cdot 10^{-7}$
10^5	6.86534	$0.6865340896048893 \cdot 10^{-8}$
10^6	2.17288	$0.2172876990443141 \cdot 10^{-8}$
10^7	0.68718	$0.6871800967015870 \cdot 10^{-9}$
10^8	0.21731	$0.2173071713839100 \cdot 10^{-9}$
10^9	0.06872	$0.6871861620664091 \cdot 10^{-10}$
10^{10}	0.02173	$0.2173073612848046 \cdot 10^{-10}$
10^{11}	0.00687	$0.6871861905921111 \cdot 10^{-11}$
10^{12}	0.00217	$0.2173072627815010 \cdot 10^{-11}$

are depicted in Figures 2 and 3. As can be seen from these figures, as the frequency of the time-harmonic current increases so current density near the outer layers of the multilayer conductor. Note the magnetic field distribution on Figure 3. For all frequencies the magnetic field steadily increases throughout the first two layers which are conductive. In the third layer which is dielectric the magnetic field decays. As for the last layer, which is a conductive layer but with the least conductivity value, the magnetic field continues to decrease for lower frequency values, whereas for larger frequencies it increases due to skin effect.

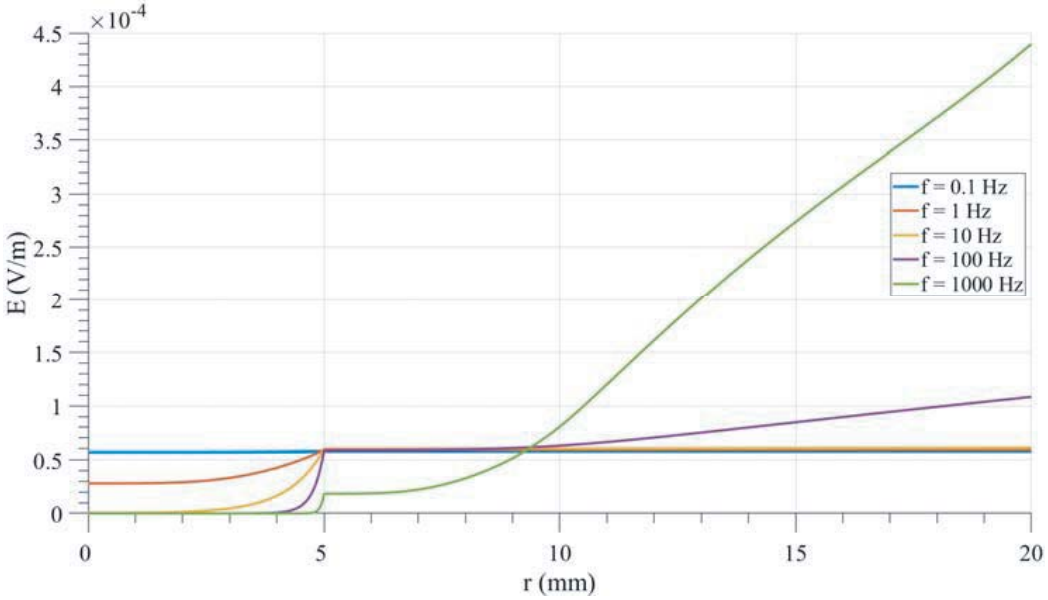

Figure 2. Distribution of electric field intensity inside a solid multilayer conductor for chosen frequency values.

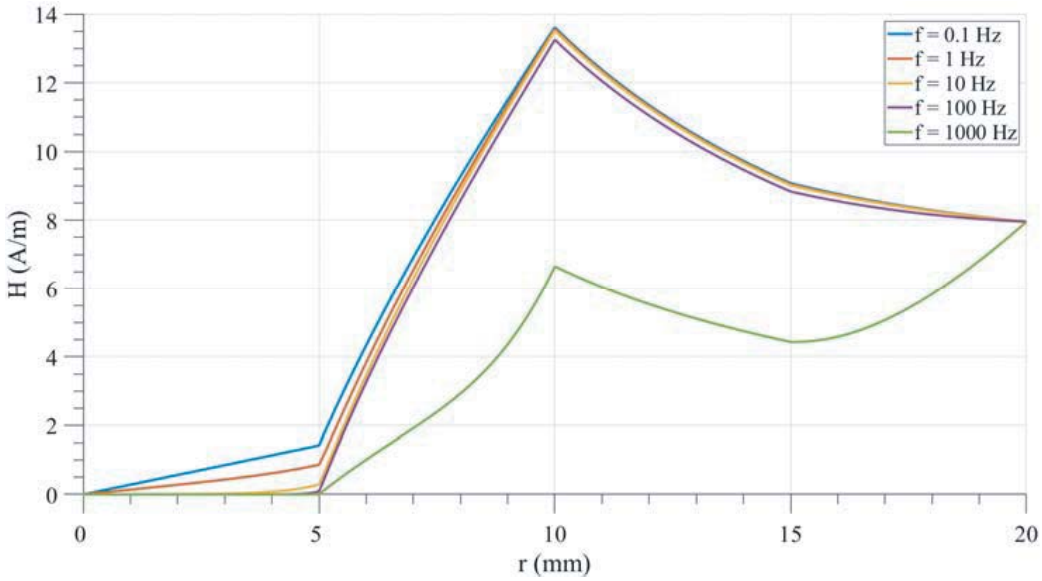

Figure 3. Distribution of magnetic field intensity inside a solid multilayer conductor for chosen frequency values.

Skin effect is also reflected on the per-unit length internal impedance of the observed multilayer cylindrical conductor. The magnitude and phase angle of the per-unit-length impedance is computed for chosen frequency values ranging from very low values to very high values and presented in Table 3.

Table 3. Per-unit length internal impedance magnitude and phase angle for a solid multilayer conductor.

f	$Z(\Omega)$	φ_z (°)
10^{-1}	$0.5775560313758815 \cdot 10^{-4}$	0.3951489094908492
10^{0}	$0.5914061365171195 \cdot 10^{-4}$	1.7347491298653899
10^{1}	$0.6081497464944294 \cdot 10^{-4}$	8.1027767611123735
10^{2}	$0.1083734518871922 \cdot 10^{-3}$	46.8628973073274295
10^{3}	$0.4399372700195623 \cdot 10^{-3}$	36.4523017889905034
10^{4}	$0.1064025308753523 \cdot 10^{-2}$	43.9140041317976397
10^{5}	$0.3346026049010050 \cdot 10^{-2}$	44.4553879063827750
10^{6}	$0.1051381045588600 \cdot 10^{-1}$	44.8300132453698978
10^{7}	$0.3318060898555213 \cdot 10^{-1}$	44.9464625345773783
10^{8}	0.1048594056779725	44.9830915686785744

6.4. Tubular Multilayer Conductor — Computation of Distribution of Electric and Magnetic Fields and Per-Unit-Length Internal Impedance

A tubular four-layer conductor is observed in this numerical example. The only difference in input data from the previous example is the internal radius of the first conductive layer $r_0 = 4\,\text{mm}$. Again, as in the previous example, distribution of electric and magnetic fields is computed in 1000 observation points inside the observed conductor for chosen frequency values. The results are depicted in Figures 4 and 5.

Per-unit length internal impedance of the observed conductor is also computed for chosen frequency values and presented in Table 4. When the values of the per-unit-length internal impedance is compared

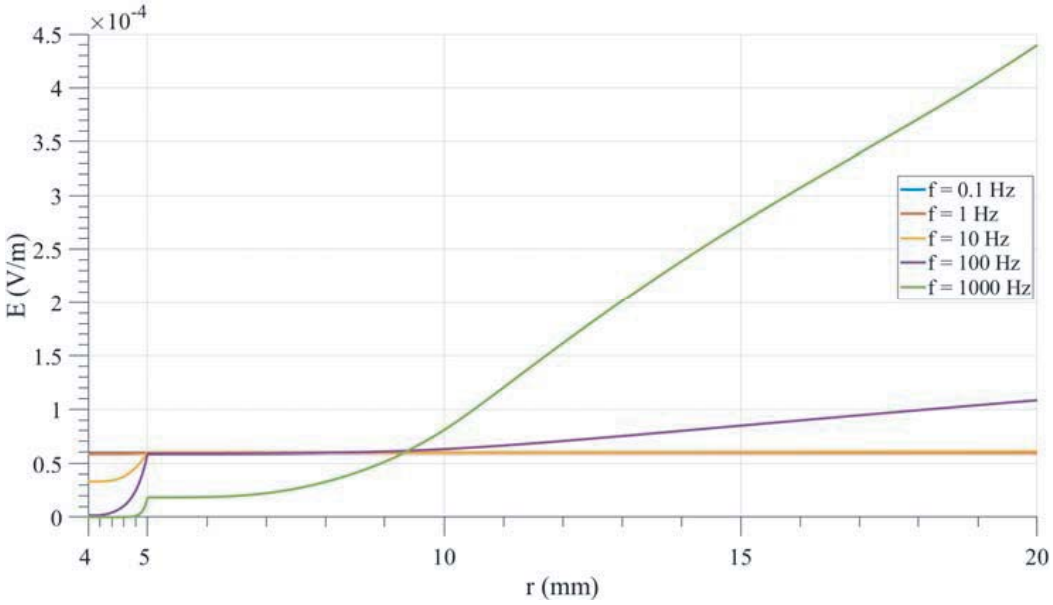

Figure 4. Distribution of electric field intensity inside a tubular multilayer conductor for chosen frequency values.

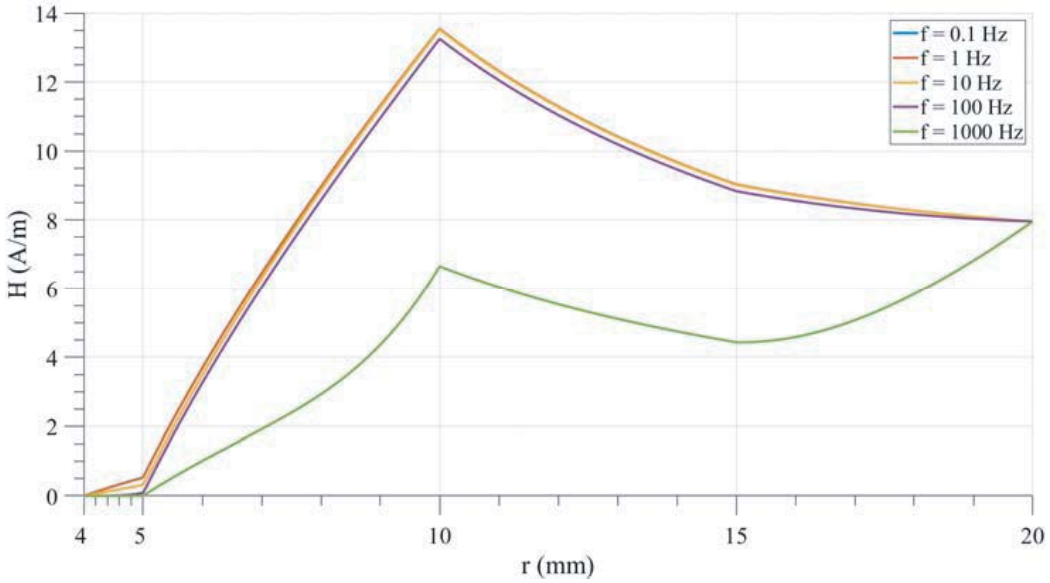

Figure 5. Distribution of magnetic field intensity inside a tubular multilayer conductor for chosen frequency values.

between the solid conductor (Table 3) and tubular conductor (Table 4), it is evident that the values are identical after the frequency value of 1 kHz which is to be expected since for larger frequencies the current density becomes larger near the surface of the conductor and the internal layers have less impact on the computed values of the internal impedance.

Table 4. Per-unit length internal impedance magnitude and phase angle for a tubular multilayer conductor.

f	$Z(\Omega)$	φ_z (°)
10^{-1}	$0.5942801604820261 \cdot 10^{-4}$	0.0908918618952423
10^{0}	$0.5945395101127369 \cdot 10^{-4}$	0.9061734998791084
10^{1}	$0.6075851098279540 \cdot 10^{-4}$	8.1354923449065240
10^{2}	$0.1083734625556642 \cdot 10^{-3}$	46.8629211428381183
10^{3}	$0.4399372700195623 \cdot 10^{-3}$	36.4523017889905034
10^{4}	$0.1064025308753523 \cdot 10^{-2}$	43.9140041317976397
10^{5}	$0.3346026049010050 \cdot 10^{-2}$	44.4553879063827750
10^{6}	$0.1051381045588600 \cdot 10^{-1}$	44.8300132453698978
10^{7}	$0.3318060898555213 \cdot 10^{-1}$	44.9464625345773783
10^{8}	0.1048594056779725	44.9830915686785744

7. CONCLUSION

In this paper a numerically robust and highly accurate algorithm for computation of electric and magnetic fields distribution inside a multilayer cylindrical conductor is presented. The multilayer conductor, which can be a solid or a tubular conductor, can consist of an arbitrary number of homogeneous layers which can have arbitrary values of electrical conductivity, permeability and permittivity. Using the computed values of electric field on the surface of the multilayer conductor, the formula for per-unit-length internal impedance is also derived. The algorithm can handle function arguments of arbitrary magnitude, which makes it suitable to use in high frequency analysis of electromagnetic phenomena.

REFERENCES

1. Schelkunoff, S. A., "The electromagnetic theory of coaxial transmission lines and cylindrical shields," *Bell System Technical Journal*, 532–578, 1934.
2. Semlyen, A. and A. Deri, "Time domain modeling of frequency dependent three phase transmission line impedance," *IEEE Transactions on Power Apparatus and Systems*, Vol. 104, No. 6, 1549–1555, 1985.
3. Wedepohl, L. M. and D. J. Wilcox, "Transient analysis of underground power transmission systems: System-model and wave propagation characteristics," *IEE Proceedings on Generation, Transmission and Distribution*, Vol. 20, No. 2, 253–260, 1973.
4. Vujević, S., V. Boras, and P. Sarajčev, "A novel algorithm for internal impedance computation of solid and tubular cylindrical conductors," *International Review of Electrical Engineering (IREE)*, Vol. 4, No. 6, Part B, 1418–1425, 2009.
5. Mingli, W. and F. Yu, "Numerical calculations of internal impedance of solid and tubular cylindrical conductors under large parameters," *IEE Proceedings — Generation, Transmission and Distribution*, Vol. 151, No. 1, 67–72, 2004.
6. Vujević, S. and D. Lovrić, "High-accurate numerical computation of internal impedance of cylindrical conductors for complex arguments of arbitrary magnitude," *IEEE Transactions on Electromagnetic Compatibility*, Vol. 56, No. 6, 1431–1438, 2014.
7. Lovrić, D. and S. Vujević, "Accurate computation of internal impedance of two-layer cylindrical conductors for arguments of arbitrary magnitude," *IEEE Transactions on Electromagnetic Compatibility*, Vol. 60, No. 2, 347–353, 2018.

8. Vujević, S., T. Modrić, and B. Vukić, "Internal impedance of two-layer cylindrical conductors," *International Review of Electrical Engineering (I.R.E.E.)*, Vol. 9, No. 1, 235–243, 2014.
9. Brandao Faria, J. A., "A circuit approach for the electromagnetic analysis of inhomogeneous cylindrical structures," *Progress In Electromagnetics Research B*, Vol. 30, 223–238, 2011.
10. Brandao Faria, J. A. M., "A matrix approach for the evaluation of the internal impedance of multilayered cylindrical structures," *Progress In Electromagnetics Research B*, Vol. 28, 351–367, 2011.
11. Kubiczek, K. and M. Kampik, "Highly accurate and numerically stable matrix computations of the internal impedance of multilayer cylindrical conductors," *IEEE Transactions on Electromagnetic Compatibility*, Early access, doi: 10.1109/TEMC.2018.2890447.
12. Stratton, J. A., *Electromagnetic Theory*, John Wiley & Sons, New Jersey, 2007.
13. Jeffrey, A. and H.-H. Dai, *Handbook of Mathematical Formulas and Integrals*, 4th Edition, Elsevier, Amsterdam, 2008.
14. Abramowitz, M. and I. A. Stegun, *Handbook of Mathematical Functions with Formulas, Graphs, and Mathematical Tables*, Dover Publications, New York, 1964.